Molecular Therapy
Original Article

Intracerebroventricular *SPAST*-AAV9 gene therapy prevents manifestation of symptoms in a mouse model of *SPG4* hereditary spastic paraplegia

Emanuela Piermarini,[1] Shrobona Guha,[1] Liang Qiang,[1] Heather Gray-Edwards,[2,3] Miguel Sena-Esteves,[2,4,5] and Peter W. Baas[1,5]

[1]Department of Neurobiology and Anatomy, Drexel University College of Medicine, 2900 Queen Lane, Philadelphia, PA 19129, USA; [2]Horae Gene Therapy Center and the Li Weibo Institute for Rare Diseases Research, UMass Chan Medical School, 381 Plantation Street, Worcester, MA, USA; [3]Department of Radiology, UMass Chan Medical School, Worcester, MA, USA; [4]Department of Neurology, UMass Chan Medical School, Worcester, MA, USA

Hereditary spastic paraplegia type 4 is characterized by gait impairments, progressive spasticity, and weakness of the lower limbs, resulting from degeneration of the corticospinal tracts. The disease is caused by mutations of the SPAST gene, which encodes a major isoform of spastin called M87 and a minor isoform called M1. Owing to its N-terminal hydrophobic domain not shared by M87, M1 is the isoform that becomes toxic when mutated. Loss of function of either M1 or M87 or both may also play a role in the disease, sensitizing corticospinal motor neurons to the toxicity of mutant M1. Here, we pursued silence-and-replace gene therapy, which addresses both gain-of-toxicity and loss-of-function components of the disease. We generated an adeno-associated serotype 9 viral vector containing microRNA to stop the expression from the endogenous SPAST gene and cDNA to express healthy human M1 and M87. The vector was introduced by intracerebroventricular injections into newborn pups of *SPAST*-C448Y, a mouse model of the disease that expresses human mutant spastin and displays adult-onset corticospinal degeneration and gait defects. The treatment successfully replaced both isoforms of endogenous spastin with healthy spastin at physiological levels, and prevented the onset and progression of corticospinal degeneration and gait defects.

INTRODUCTION

Hereditary spastic paraplegia (HSP) is a heterogeneous group of neurodegenerative disorders, resulting mainly in degeneration of the corticospinal tracts (CSTs), with other tracts also afflicted in some patients.[1–3] With a growing number of genes involved, more than 90 loci, all HSPs are characterized by progressive spasticity, muscle weakness of the lower limbs, and subsequent gait dysfunction.[4] Pathological mutations occurring in the SPAST gene result in HSP type 4, also called *SPG4*-HSP, which represents the most common form of the known HSPs, accounting for roughly 40% of the cases, either familial or sporadic.[1,5] More than 200 different pathogenic mutations have been identified in the *SPAST* gene, including truncating types and missense variants. To date, there are no approved therapies for patients with *SPG4*-HSP beyond strategies to make the symptoms more tolerable. Management is limited mainly to physical therapy and, for some patients, Botox to reduce muscle spasticity.

Spastin presents as two main isoforms: a longer one called M1 (68 kDa) and a slightly shorter one (61 kDa) called M87. In rodents, M87 is called M85 (due to minor sequence differences), but for simplicity we refer to it as M87, regardless of species. Over the past few years, studies from our laboratory have provided evidence for a gain-of-toxicity mechanism as necessary and sufficient for *SPG4*-HSP, with loss of function of M1, M87, or both as an exacerbating factor.[6,7] Our studies, conducted on various cellular and invertebrate models, show that M1 acquires toxic properties when mutated, while M87 does not.[8] Building on this work, we generated a mouse model, named *SPAST*-C448Y, in which SPAST cDNA with the missense C448Y mutation was inserted into the *ROSA26* locus.[9] This mouse displays adult-onset gait deficiencies and CST dieback degeneration, reminiscent of the human disease, and the symptoms are worsened in the offspring of this mouse crossed with a *Spast* knockout mouse.[10]

In recent years, we have focused on how to mitigate the toxicity of the mutant M1,[6,9] which available evidence suggests accumulates in the CSTs, while other investigators have focused on how to compensate for lost spastin function.[11,12] Theoretically, a classic silence-and-replace gene therapy approach would accomplish both, turning off

Received 14 April 2025; accepted 19 November 2025;
https://doi.org/10.1016/j.ymthe.2025.11.029.

[5]Senior authors

Correspondence: Emanuela Piermarini, Department of Neurobiology and Anatomy, Drexel University College of Medicine, 2900 Queen Lane, Philadelphia, PA 19129, USA.
E-mail: ep477@drexel.edu
Correspondence: Peter W. Baas, Department of Neurobiology and Anatomy, Drexel University College of Medicine, 2900 Queen Lane, Philadelphia, PA 19129, USA.
E-mail: pwb22@drexel.edu

Please cite this article in press as: Piermarini et al., Intracerebroventricular *SPAST*-AAV9 gene therapy prevents manifestation of symptoms in a mouse model of *SPG4* hereditary spastic paraplegia, Molecular Therapy (2025), https://doi.org/10.1016/j.ymthe.2025.11.029

expression from the endogenous SPAST genes and replacing their expression with that from a healthy SPAST gene.

Since gene therapy was conceptualized a few decades ago,[13–15] the technology has advanced, with positive indications of tolerability and effectiveness for various neurological disorders.[16–19] In particular, adeno-associated virus (AAV) vectors, especially AAV serotype 9, have proven effective in transducing a wide variety of tissues, including central nervous system (CNS) tissues,[20] leading to stable transgene expression,[21–24] and presenting a favorable clinical safety profile.[25] Several strategies have been developed to access the CNS, including intraparenchymal injections,[26–28] injection of the vector into cerebroventricular space,[29–31] intrathecal administration into the cisterna magna or the lumbar area,[32–34] and intravenous injection.[35,36] Direct vector injection into the CNS is invasive but also more effective at transducing larger areas of the brain than other routes, especially when administered intracerebroventricularly (ICV).

There are challenges associated with gene therapy for *SPG4*-HSP. M1 is produced by expression from a weak/leaky start codon, presumably evolved to ensure that protein levels remain extremely low.[37,38] An excess of wild-type (WT) M1 would likely be as pathogenic as mutant M1. However, M87 is a strong microtubule-severing protein,[8,39,40] too much of which would destroy the microtubule array of the transduced cells and likely kill them. Mutant M1 becomes resistant to degradation,[8,12,41,42] so a patient with many years of accumulation of mutant M1 may continue to suffer its ill effects, despite the inhibition of expression of more. As with most diseases, gene therapy is best suited to prevent the symptoms from occurring if introduced pre-symptomatically or to prevent the symptoms from worsening if introduced symptomatically.

Here, in the first pre-clinical investigation of gene therapy for *SPG4*-HSP, we evaluated the therapeutic efficacy of a dual AAV9 vector, named *SPAST*-AAV9, comprising a microRNA (miRNA or miR) and cDNA of WT human SPAST (modified to be unaffected by the miRNA). We administered the vector using ICV injections into neonatal *SPAST*-C448Y mice. Once the animals became adults, we ascertained the impact of the vector on the expression levels of WT M1 and M87, the health status of their CSTs, and their gait behavior, all relative to both WT and non-injected *SPAST*-C448Y mice. A safety profile based on a clinical chemistry panel was also generated.

RESULTS

Generation of M1-specific antibodies

M1 and M87 are produced by the same mRNA via separate start codons. M87 is ubiquitously expressed in all tissues, while M1 is only detected in brain and spinal cord.[43] These two isoforms share all of the same domains except for the N-terminal domain that is specific to M1 (N-Term, Figure 1A). M87 and M1 are functionally distinct, with M87 serving as a microtubule-severing enzyme[8,39,40] and M1 playing a role in shaping the internal membranes of cells.[12,44–47] M1 levels are extremely low compared to M87, with M1 barely (if at all) detectable in most tissues with available tools. This is mainly because M87 is expressed from a strong start codon, while M1 is expressed from a weak start codon that presumably evolved to ensure that M1 levels remain low in cells.[37,48,49] Other regulatory mechanisms also contribute to the relative levels of the two isoforms.[49,50]

When a mutation exists in the *SPAST* gene, both M1 and M87 bear the mutation, but only mutant M1 is cytotoxic and only mutant M1 becomes resistant to degradation.[8,43,50] Mutant M87 is dysfunctional but not cytotoxic or resistant to degradation. In support of this, a prominent band corresponding to accumulated M1 was observed on the western blot (WB) of the spinal cord from a human patient with a truncating SPAST mutation yielding spastin proteins lower in molecular weight than their WT counterparts.[43] A confounding unknown is the role of haploinsufficiency in the disease and the degree to which effective gene therapy must also restore physiological levels of M1, M87, or both, in addition to ridding the neurons of mutant M1. The critical importance of investigating both spastin isoforms has long been problematic because there are no tools to distinguish these two isoforms, and M1 is present at such vanishingly low levels. Recognizing the limitations of available commercial spastin antibodies, we generated new M1-specific polyclonal antibodies as a critical component of the present study, aiming to enable more accurate and reliable detection of M1 alongside the development and testing of the gene therapy vector.

Commercially available spastin antibodies recognize both M1 and M87 and hence cannot distinguish them on immunocytochemical or immunohistochemical preparations.[51,52] On WB with these antibodies, M87 appears as a prominent band, whereas M1 is undetectable in most tissues. M1 becomes apparent in the adult spinal cord as a minor band with slightly greater molecular weight than M87.[49] Using as antigen the first 28 amino acids (aa) specific to M1 to avoid its most hydrophobic region, we generated polyclonal antibodies in rabbit (Figure 1B). We found through a series of validation experiments that the antibodies are highly specific to M1 and sensitive enough to detect endogenous human and mouse M1 in our mouse model, thus serving our purposes.

The antibodies recognize human M1 ectopically expressed in neuroblastoma cells but not human M87 similarly ectopically expressed, with no prominent non-specific bands (Figure 1C). This was also the case for mouse and rat spastin proteins. In all cases, ectopically expressed M1 and M87 were both recognized by a general spastin antibody. Moreover, in the spinal cord, an M1 band is apparent in WT and *SPAST*-C448Y$^{+/-}$ mice that is not present in the spinal cord of the homozygous knockout mouse (*Spast*$^{-/-}$), confirming the antibody's specificity (Figures 1D and 1E).

Generation of the *SPAST*-AAV9 dual vector

Because the *SPAST*-C448Y mouse expresses both WT mouse spastin and human mutant spastin, an miRNA for SPAST (miR^{SPAST}) was chosen to target both of them. The U6 promoter, standard for

Please cite this article in press as: Piermarini et al., Intracerebroventricular *SPAST*-AAV9 gene therapy prevents manifestation of symptoms in a mouse model of *SPG4* hereditary spastic paraplegia, Molecular Therapy (2025), https://doi.org/10.1016/j.ymthe.2025.11.029

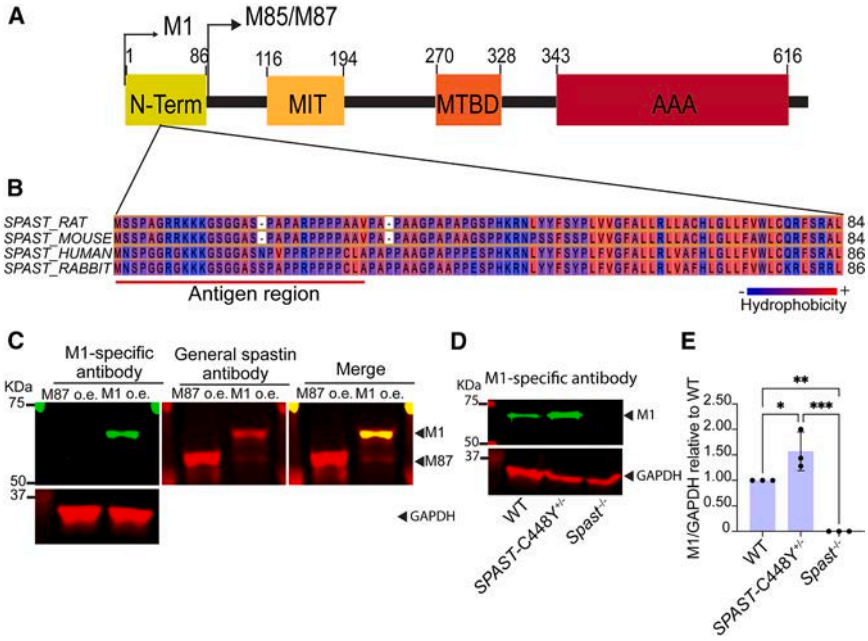

Figure 1. Generation of M1-specific rabbit polyclonal antibodies

(A) Schematic illustration of spastin protein domains. M1 and M85/M87 start codons are highlighted. N-Term, N-terminal; MIT, microtubules interacting and trafficking domain; MTBD, microtubule binding domain; AAA, ATPase associated with various cellular activities. (B) The alignment of the N-Term domain among different species is conserved. The first 28 aa, which is the least hydrophobic region of the N-Term domain, were used to design the M1-specific antibody. (C) HEK293T cells ectopically expressing M87 or M1 are probed with M1-specific antibody and general spastin antibody. The merge image shows overlapping of M1-spastin bands for M1 antibody and general spastin antibody. o.e., overexpression. (D) Spinal cord tissue lysates from WT, *SPAST*-C448Y$^{+/-}$, and *Spast*$^{-/-}$ mice at 6 months of age, showing prominent band in the former but not the latter. No other bands of any prominence were observed anywhere along the full length of the blots (only a portion of which is shown here). (E) Quantifications of M1 levels were normalized to GAPDH relative to WT. Data are represented as mean ± SD, with WT values normalized to 1. For statistical tests, one-way ANOVA with Tukey post hoc analysis was conducted. $^{*}p = 0.04$; $^{**}p = 0.003$; $^{***}p < 0.001$.

miRNA expression, was chosen to drive the miR^{SPAST}. As for the cDNA component, alterations were introduced in the third nucleotide (known as the wobble position) of codons overlapping the seed sequence to be resistant to the miRs, while keeping the fidelity of the sequence of the protein. The Mecp2 promoter was selected for its compact size, which allows for larger transgenes to be packaged in AAV vectors, and because it effectively drives gene expression, with specificity, in neurons within the CNS.[53] Additionally, the Mecp2 promoter has already been successfully documented in driving the DNA component for gene therapy vectors targeting brain cells.[54,55] Plasmids containing either the miRNA for SPAST (miR^{SPAST}) or the cDNA were transfected into HEK293T cells ectopically expressing human or mouse M1 or M87. With satisfactory results obtained for both component parts (data not shown), we combined them into a gene therapy AAV9 dual vector (with AAV9 chosen as the viral vector for transduction for reasons outlined in the introduction) termed *SPAST*-AAV9 (shown schematically in Figure 2A). For the *in vivo* experiments, P0 (postnatal day 0)/P1 animals were either non-injected or injected via ICV injections of the *SPAST*-AAV9 vector at a dose of 2.0×10^{10} vg/mouse, with a total volume of 2 μL each ventricle. No signs of trauma or leakage were observed at the injection site, and general histological assessments of the surrounding tissue revealed no abnormalities indicative (vg, viral genomes) of injection-induced damage. No sham-injected group was included in our studies as control (Figure 2B).

ICV delivery of *SPAST*-AAV9 vector silences and replaces endogenous SPAST genes in *SPAST*-C448Y mice

SPG4-HSP primarily affects upper motor neurons and the long axons they extend to form the CST, but it also affects other tracts in many patients to varying degrees. Therefore, the more widespread the transduction of neurons, the better. Additionally relevant is the fact that overcoming degeneration that has already occurred is a much greater challenge than preventing the degeneration from occurring. For these reasons, we chose for our first gene therapy studies to use ICV injection of P0/P1 pups, which permits a broad distribution of the vector across the CNS and theoretically enables the vector to duplicate the phenotype of the WT animal. P0/P1 mice were injected intracerebroventricularly with 2.0×10^{10} vg/mouse of *SPAST*-AAV9 vector, for a total of 2 μL each ventricle, using stereotaxic coordinates: approximately 1 mm anterior-posterior to bregma (AP); +1 mm medial-lateral from midline (ML); and 2 mm depth from the skin surface (DV). This delivery method targets the cerebrospinal fluid, bypassing the blood-brain barrier.[56,57] To verify that the spastin detected via WB resulted from the cDNA in the vector rather than representing endogenous protein not depleted by the miR^{SPAST}, we conducted an additional experiment using homozygous spastin knockout mice (*Spast*$^{-/-}$), which do not show any spastin bands on WB.[58] WT and *Spast*$^{-/-}$ male and female mice were ICV injected at P0 with the *SPAST*-AAV9 vector.

Given that *SPG4*-HSP primarily affects the long descending axons of the CSTs, which reside in the spinal cord, we focused our analysis of spastin expression in this region. Degeneration of these axons is a defining feature of the disease and is closely linked to the progressive motor symptoms observed in both patients and mouse models. Assessing spastin levels in the spinal cord therefore provides a direct and disease-relevant measure of the silencing and replacement efficacy of the *SPAST*-AAV9 vector. Thus, at 3 months post-injection, 3 animals from each group (non-injected versus *SPAST*-AAV9 injected) were sacrificed, and spastin levels were evaluated in spinal

Please cite this article in press as: Piermarini et al., Intracerebroventricular *SPAST*-AAV9 gene therapy prevents manifestation of symptoms in a mouse model of *SPG4* hereditary spastic paraplegia, Molecular Therapy (2025), https://doi.org/10.1016/j.ymthe.2025.11.029

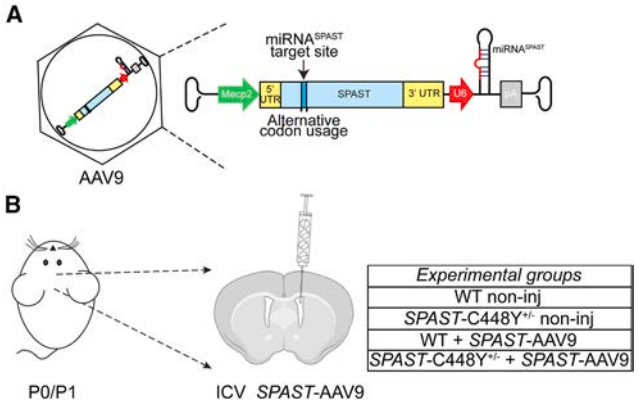

Figure 2. Generation of the *SPAST*-AAV9 vector

(A) A dual vector was generated to silence-and-replace endogenous M1 and M87 mutated spastin with healthy spastin isoforms. The vector presents a miR^{SPAST} under U6 promoter to efficiently knock down spastin, while *SPAST*-cDNA expression was achieved using a Mecp2 promoter. The target sequence in the *SPAST*-cDNA has been altered at the third nucleotide of codons, known as the wobble position, so that *SPAST*-cDNA is miR resistant. (B) Schematic overview of the ICV injection. The *SPAST*-AAV9 was stereotactically injected into the cerebral ventricles of P0/P1 pups of WT and *SPAST*-C448Y$^{+/-}$ mice. Non-injected animals were used as the control group.

cord tissues (Figures 3A–3C). Levels of M1 and M87 were then determined in the CNS tissues (motor cortex and spinal cord) of WT and *SPAST*-C448Y$^{+/-}$ using the M1-specific polyclonal antibody and a general spastin antibody to detect M87 (Figures 3D and 3G, respectively). WB results are consistent with effective silence-and-replace. The non-injected *SPAST*-C448Y$^{+/-}$ animals had higher levels of both M1 and M87 than WT in the motor cortex (Figures 3E and 3F) and spinal cord tissues (Figures 3H and 3I). In both the motor cortex and spinal cord tissues of WT+*SPAST*-AAV9 animals, M87 levels appear to be slightly elevated compared to WT non-injected animals, while M1 levels remained similar. This likely reflects the low endogenous expression of M1 in adult cortex and may indicate a limited dynamic range for detecting changes in M1. It is also possible that the expression of the SPAST cDNA favors M87 production, contributing to the observed isoform-specific differences.

Spastin is not a neuron-specific protein and is normally also expressed in peripheral tissues. In our genetic mouse model, human mutant spastin is ubiquitously expressed in peripheral organs, such as the liver.[9] This provided an opportunity to validate the dual-function design of our vector, demonstrating that the miRNA effectively silences endogenous SPAST, while the replacement cDNA restores expression to control levels, but only in neurons. While the vector uses a neuron-selective Mecp2 promoter for the DNA, the possibility remains that spastin may be silenced in peripheral tissues without sufficient replacement, potentially leading to depletion-related effects. As shown in Figure 4, M87 in the liver was almost completely depleted, with no detectable replacement of the depleted protein, consistent with efficient miRNA-mediated silencing of the endogenous SPAST genes but without expression of the cDNA via the neuron-specific Mecp2 promoter (Figure 4B). While this is strong evidence that the vector is working as expected, potential consequences of depleting organs such as the liver of their spastin but not replacing it will need further consideration.

SPAST-AAV9 produced no observable adverse effects in *SPAST*-C448Y mice

To test whether treatment with *SPAST*-AAV9 leads to organ toxicity in *SPAST*-C448Y$^{+/-}$ mice, mouse sera were collected, and a full blood chemistry panel was analyzed, including aspartate transaminase (AST), alanine transaminase (ALT), total bilirubin (T.Bil), albumin, total proteins (T.Pro), creatinine (CREA), and electrolytes (Na, K, Cl), as shown in Figure 5A. Animals receiving *SPAST*-AAV9 at 2.0×10^{10} vg/mouse had overall normal levels of these serum markers at 6 months post-injection, with no significant differences in liver function (Figures 5B–5E) or kidney function (Figure 5F), although we noticed elevated AST and T.Bil levels in the WT+*SPAST*-AAV9 group compared to the WT non-inj(WT non-injected) group. Importantly, this slight elevation observed in both parameters appeared to be driven primarily by a single animal, and all values remained within reference ranges for healthy animals not typically associated with overt liver toxicity in mice.

Interestingly, CREA levels were significantly lower in the *SPAST*-C448Y$^{+/-}$, consistent with muscle deterioration,[59,60] with *SPAST*-AAV9 treatment restoring CREA levels to WT (Figure 5G). No significant differences were detected in electrolytes, as indicated for Na, K, and Cl graphs in Figures 5H–5J, which is important because the body depends on adequate intake of nutrients, proper absorption of nutrients by the intestines, and proper kidney and lung function. These results demonstrate that the *SPAST*-C448Y$^{+/-}$ mice tolerated the *SPAST*-AAV9 vector well.

SPAST-AAV9 vector prevents axons from degenerating when introduced into pre-symptomatic *SPAST*-C448Y mice

In mice, the CST is located mainly in the dorsal columns (>95%), with a very small fraction existing in the ventral column[61,62] (Figure 6A). Quantitative evaluation of the extent of axonal degeneration was carried out in the dorsal column from the spinal cords of all 4 groups. Two different types of analysis were conducted, similar to our recently published articles,[9,10] with the ratio of axon numbers at the lumbar level versus those at the cervical level indicating the degree of axonal dieback degeneration. Axonal degeneration is also reflected as changes in the phosphorylation status of the neurofilaments in various neurodegenerative diseases.[63,64] The *SPAST*-C448Y$^{+/-}$ mice display increased phospho-neurofilament compared to WT (Figures 6B and 6C) at the dorsal column of the lumbar level, using SMI312 as marker, suggesting that the CST is degenerating. Of note, *SPAST*-C448Y$^{+/-}$ + *SPAST*-AAV9 presented the same level of phospho-neurofilament as WT (Figure 6C). To determine whether the *SPAST*-AAV9 vector had an effect on axonal preservation, we quantified SMI311^{+} axons in both cervical and lumbar dorsal columns of the spinal cord. The analysis using the total neurofilament staining SMI311 revealed reduced axonal count at the lumbar level

Please cite this article in press as: Piermarini et al., Intracerebroventricular *SPAST*-AAV9 gene therapy prevents manifestation of symptoms in a mouse model of *SPG4* hereditary spastic paraplegia, Molecular Therapy (2025), https://doi.org/10.1016/j.ymthe.2025.11.029

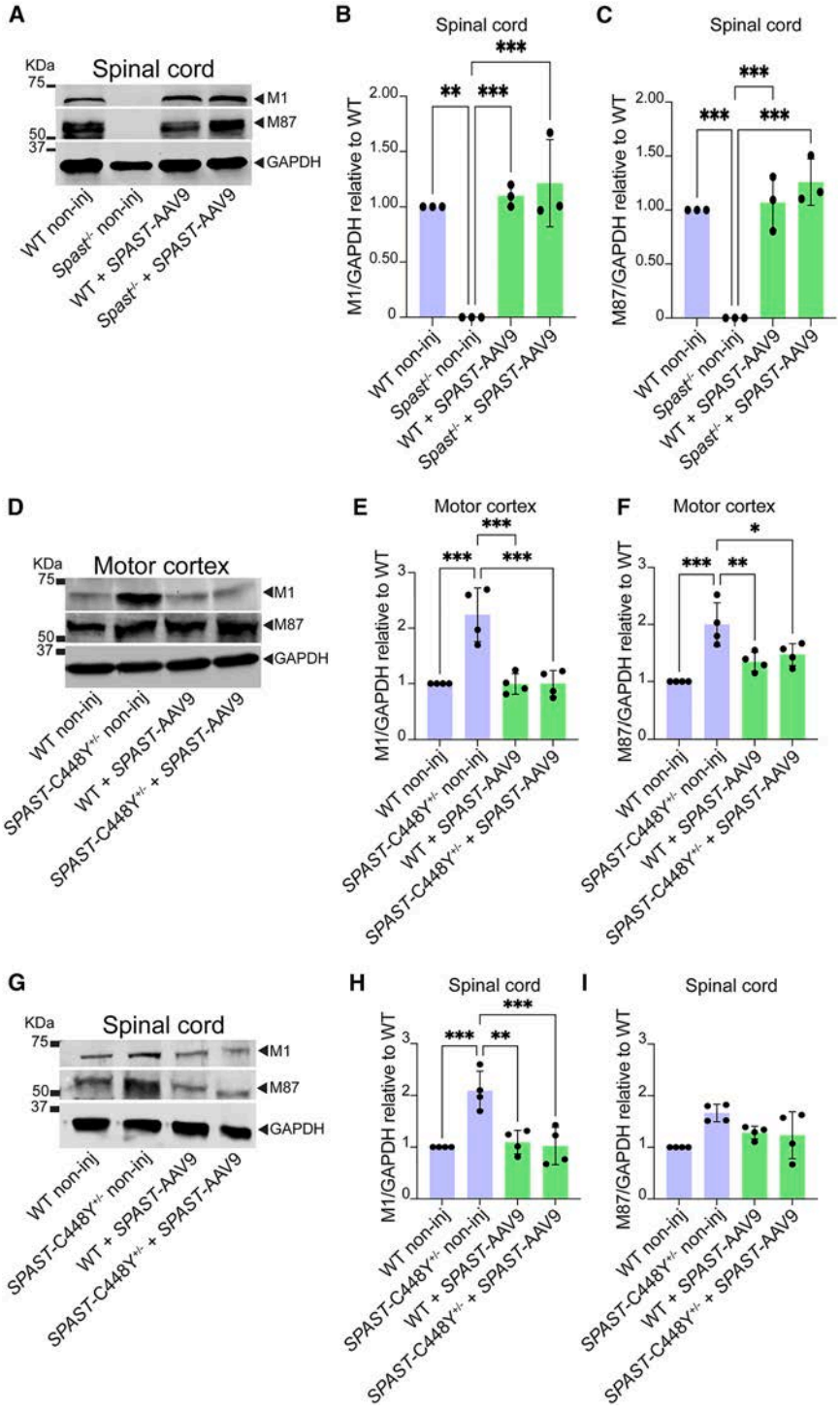

Figure 3. Evaluation of M1 and M87 spastin protein levels in the motor cortex and spinal cord

(A) Representative WB of the spinal cord lysates from WT and *Spast*$^{-/-}$ mice at 3 months either non-injected or *SPAST*-AAV9-injected probed for M1-specific and general spastin antibodies. (B and C) (B) Quantifications of M1 and (C) M87 levels in the spinal cord for WT non-inj, *Spast*$^{-/-}$ non-inj, WT+*SPAST*-AAV9, and *Spast*$^{-/-}$+*SPAST*-AAV9 mice. Quantifications of spastin intensity were normalized to GAPDH relative to WT. Data are represented as mean ± SD, with WT values normalized to 1. For each experimental group, lysates were collected from 3 mice, 2 males and 1 female. For statistical tests, one-way ANOVA with Tukey post hoc analysis was conducted. $^{**}p = 0.001$; $^{***}p < 0.001$. (D) Representative WB of motor cortex from WT and *SPAST*-C448Y$^{+/-}$ mice collected at 6 months of age either non-injected or *SPAST*-AAV9 injected. (E and F) (E) Quantifications of M1 and (F) M87 levels in the motor cortex for WT non-inj, *SPAST*-C448Y$^{+/-}$ non-inj, WT+*SPAST*-AAV9, and *SPAST*-C448Y$^{+/-}$+*SPAST*-AAV9 mice. Quantifications of spastin intensity were normalized to GAPDH relative to WT. Data are represented as mean ± SD, with WT values normalized to 1. For statistical tests, one-way ANOVA with Tukey post hoc analysis was conducted. $^{*}p = 0.03$; $^{**}p = 0.008$; $^{***}p < 0.001$. (G) Representative WB of spinal cord from WT and *SPAST*-C448Y$^{+/-}$ mice collected at 6 months of age either non-injected or *SPAST*-AAV9 injected. (H and I) (H) Quantifications of M1 and (I) M87 levels in the spinal cord at 6 months of age for WT non-inj, *SPAST*-C448Y$^{+/-}$ non-inj, WT+*SPAST*-AAV9, and *SPAST*-C448Y$^{+/-}$+*SPAST*-AAV9 mice. Quantifications of spastin intensity were normalized to GAPDH relative to WT. Data are represented as mean ± SD, with WT values normalized to 1. For each experimental group, lysates were collected from 4 mice, 2 males and 2 females. For statistical tests, one-way ANOVA with Tukey post hoc analysis was conducted. $^{*}p = 0.01$; $^{**}p = 0.002$; $^{***}p < 0.001$.

compared to the cervical level in the *SPAST*-C448Y$^{+/-}$ mice relative to WT, further confirming degeneration via axonal dieback in the CST (Figure 6D). Importantly, *SPAST*-AAV9-treated mice showed a significant rescue of axonal density in the lumbar region (Figure 6D, green bars). These results indicate that treatment with *SPAST*-AAV9 prevents the axonal dieback degeneration in the *SPAST*-C448Y$^{+/-}$ mouse model for up to 6 months after a single injection of the vector at the pre-symptomatic age.

SPAST-AAV9 prevents gait alterations from occurring when introduced into pre-symptomatic *SPAST*-C448Y mice

Motor and coordination dysfunction, including gait abnormalities, are the main diagnostic criteria for many neurodegenerative disorders. Therefore, various behavioral experiments to assess motor deficits are used in rodent models[65,66] and provide a reliable and quantifiable readout of the effectiveness of therapeutic strategies. *SPAST*-C448Y$^{+/-}$ mice displayed gait abnormalities in the beam walk assay, hindlimb clasping, and CatWalk assay, and these

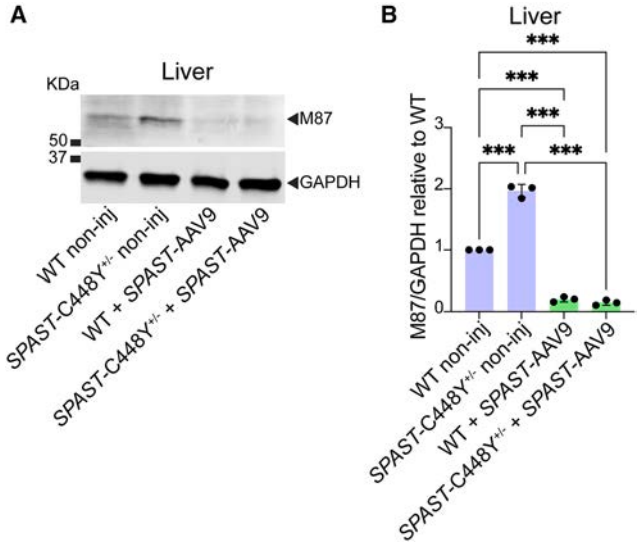

Figure 4. Evaluation of M87 spastin protein levels in the liver

(A) Representative WB of liver lysates from WT and *SPAST*-C448Y$^{+/-}$ mice at 6 months either non-injected or *SPAST*-AAV9 injected probed with the general spastin antibodies to detect M87. (B) Quantifications of M87 levels in the liver for WT non-inj, *SPAST*-C448Y$^{+/-}$ non-inj, WT+*SPAST*-AAV9, and *SPAST*-C448Y$^{+/-}$-+*SPAST*-AAV9 mice. Quantifications of spastin intensity were normalized to GAPDH relative to WT. Data are represented as mean ± SD, with WT values normalized to 1. For each experimental group, lysates were collected from 3 mice, 2 males and 1 female. For statistical tests, one-way ANOVA with Tukey post hoc analysis was conducted. ***$p < 0.001$.

abnormalities are consistent with CST degeneration in *SPG4*-HSP patients.[9,10]

To test whether the *SPAST*-AAV9 gene therapy improves behavioral defects in *SPAST*-C448Y$^{+/-}$ mice, a mouse cohorts of 8–12 animals per group, with equal numbers of males and females, underwent a battery of behavioral tests using CatWalk. The CatWalk apparatus is an automated system that provides user-independent quantitative assessments of multiple spatiotemporal parameters.[67] It is one of the most detailed and sensitive assays for detecting gait defects and locomotor functions, with over 90 different gait parameters that can be assessed. This test was originally selected based on the neurological phenotypes in *SPAST*-C448Y$^{+/-}$ mice and because it can be repeated longitudinally.[10] Mice are filmed by a high-speed camera from underneath while traversing through a walkway. When the animal's paws contact the glass, the light is scattered, and digital images of the paws are produced by the software that labels paw prints so that gait parameters can be assessed. We primarily focused on stand duration, swing duration, cadence, and print width, based on their correlation with the parameters used to assess gait alterations in human *SPG4*-HSP patients.[68] These studies were performed on all the mice, WT and *SPAST*-C448Y$^{+/-}$, either non-injected or *SPAST*-AAV9 injected, and gait analyses were recorded at 3 and 6 months of age to assess disease progression and to evaluate the therapeutic effects of the *SPAST*-AAV9 vector (Figure 7A). The 3-months time point corresponds to the onset of gait deficits in the *SPAST*-C448Y$^{+/-}$ mice, allowing analysis of early-stage pathology, while the 6-month time point represents a more advanced disease stage, with pronounced functional impairments and axonal degeneration. This design enabled evaluation of both short- and mid-term efficacy of the *SPAST*-AAV9 gene therapy approach and provided a broader understanding of treatment response over time in the disease model.

The *SPAST*-C448Y$^{+/-}$ non-injected group shows significant gait deficiencies in stand and swing duration at 3 months of age when compared to WT (Figures 7B and 7C), while no significant differences were detected for cadence (Figure 7D) or print width (Figure 7E). At 6 months of age, the behavioral phenotype progresses, with all the parameters worsening in the *SPAST*-C448Y$^{+/-}$ non-inj (Figures 7F–7I). Of note, *SPAST*-C448Y$^{+/-}$ mice injected at pre-symptomatic age with the *SPAST*-AAV9 were indistinguishable from WT at 3 and 6 months post-injection regarding all parameters. Thus, the *SPAST*-AAV9 vector entirely prevented the degenerative phenotype otherwise displayed by the *SPAST*-C448Y$^{+/-}$ mice at both 3 and 6 months of age.

DISCUSSION

There has been controversy in the field as to whether *SPG4*-HSP is caused mainly by a loss-of-function or a gain-of-toxicity disease pathway,[7,9–11,41–43,69–71] but the strength of a classic gene therapy approach is that both possibilities are addressed. Theoretically, if all cells relevant to the disease can be transduced prior to the onset of the pathology, the nerve degeneration and associated symptoms should be completely avoided. Our present study demonstrate success in achieving that outcome by introducing into newborn mice an AAV9-driven silence-and-replace vector. In achieving such an outcome, not only must the miRNA be highly effective but, especially in the case of spastin (compared with many other HSP-related proteins), the levels of replacement protein must be sufficient but not too high. M87 is a potent microtubule-severing enzyme that would destroy the microtubule array of the transduced cells if expressed at levels too high to be appropriately regulated. In the case of M1, whose mutant form is the primary cause of the disease as indicated by several studies,[7,9] the normal levels are vanishingly small, probably because any higher levels would have adverse effects, presumably similar to the mutant versions. While a shortcoming of WB analyses is that they combine transduced and un-transduced cells, the results, taken collectively, suggest that the miR^{SPAST} is effective and that the cDNA expresses physiological levels of M1 and M87. This would seem to be ideal, as reflected in the positive outcome of the histology and behavioral analyses of the animals as they age. In addition, there are no indications of significant toxicity of the vector from blood chemistry panels.

One limitation of the present study is that blood samples for serum chemistry were collected only at the 6-month time point, with the goal of assessing long-term safety and tolerability of *SPAST*-AAV9 treatment. While this approach captures chronic effects, it may overlook transient elevations in toxicity markers that could occur shortly

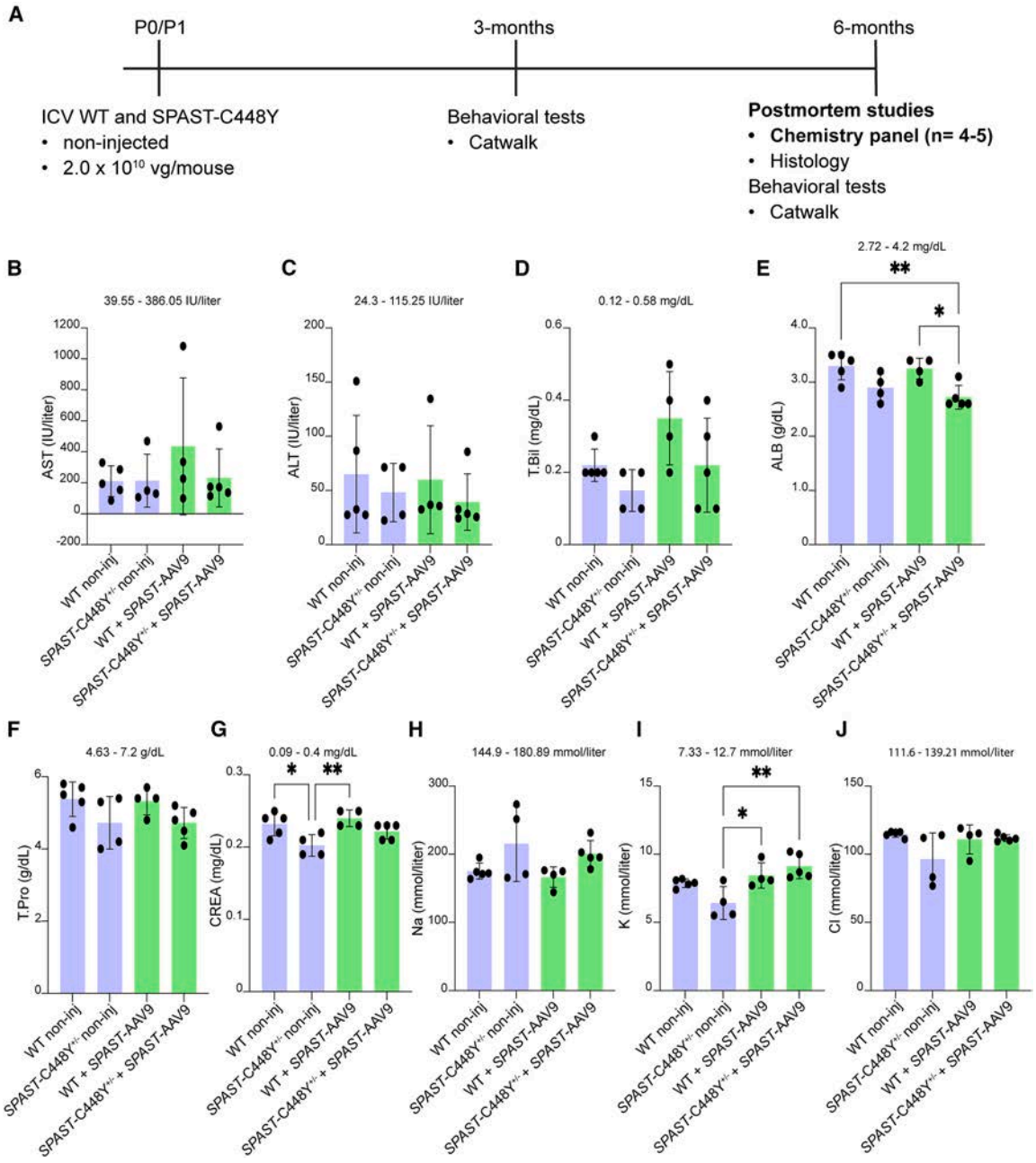

Figure 5. Serum chemistry panel indicates no significant adverse effects of ICV *SPAST*-AAV9

(A) Non-injected or 2.0 × 10^{10} vg/mouse of *SPAST*-AAV9 vector was administered intracerebroventricularly (ICV) at P0/P1 to an equal number of males and females from WT and *SPAST*-C448Y$^{+/-}$ mice. At 6 months, animals were assessed for behavioral tests and sacrificed for postmortem studies, including serum chemistry panel and histological analyses. (B–J) No significant differences were observed, with the exception of the CREA parameter (G). (E) For statistical tests, one-way ANOVA with Tukey post hoc analysis was conducted. *$p = 0.02$; **$p = 0.007$. (G) For statistical tests, one-way ANOVA with Tukey post hoc analysis was conducted. *$p = 0.03$; **$p = 0.008$. (I) For statistical tests, one-way ANOVA with Tukey post hoc analysis was conducted. *$p = 0.02$; **$p = 0.002$. AAV9, adeno-associated virus 9; ALB, albumin; ALT, alanine transaminase; AST, aspartate transaminase; Cl, chloride; CREA, creatinine; K, potassium; Na, sodium; T.Bil, total bilirubin; T.Pro, total proteins. The reference values of each parameter are reported above the corresponding graph. Each data point represents a measurement from an individual animal, with bars representing the mean ± SD. WT non-inj $n = 5$, *SPAST*-C448Y$^{+/-}$ non-inj $n = 4$, WT+*SPAST*-AAV9 $n = 4$, and *SPAST*-C448Y$^{+/-}$+*SPAST*-AAV9 $n = 5$.

Please cite this article in press as: Piermarini et al., Intracerebroventricular *SPAST*-AAV9 gene therapy prevents manifestation of symptoms in a mouse model of *SPG4* hereditary spastic paraplegia, Molecular Therapy (2025), https://doi.org/10.1016/j.ymthe.2025.11.029

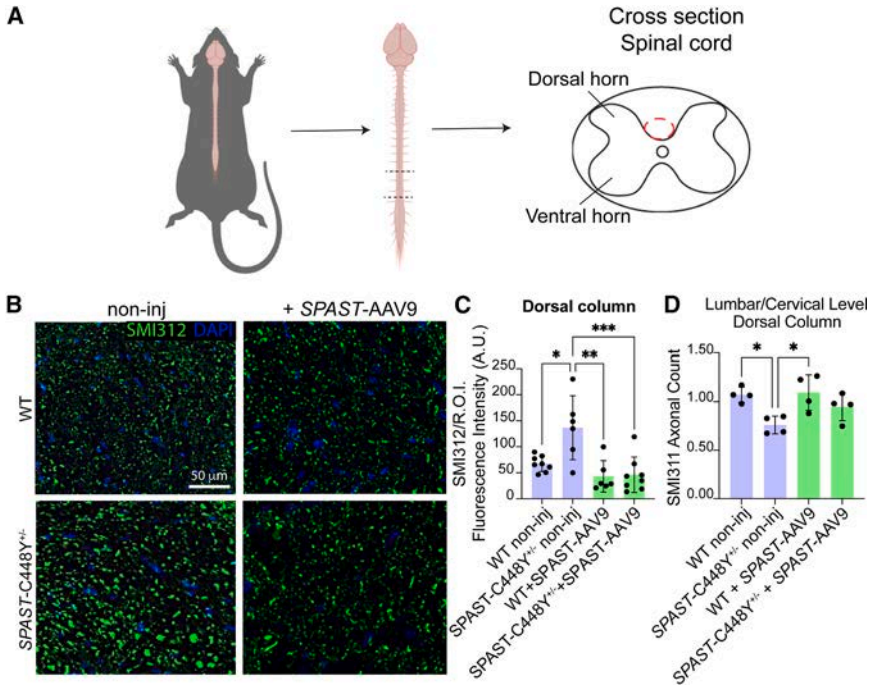

Figure 6. ICV of *SPAST*-AAV9 prevents axonal degeneration in *SPAST*-C448Y$^{+/-}$

(A) Mice from all experimental groups were perfused in 4% PFA at 6 months of age, and brain and spinal cord were dissected. (B) Representative enlarged cross-sections of the dorsal column at the lumbar level of the spinal cord, stained with SMI312 to assess changes in neurofilament phosphorylation status in the CST within the region of interest (ROI). (C) Quantification shows increased SMI312 fluorescence intensity in *SPAST*-C448Y$^{+/-}$ non-inj compared to WT non-inj, while the presymptomatic injection of the *SPAST*-AAV9 prevents the degeneration from occurring. Data are represented as mean ± SD. Each data point is an average of 5–12 randomly selected sections from 1 animal. For SMI312 staining, WT non-inj n = 8, *SPAST*-C448Y$^{+/-}$ non-inj n = 6, WT+*SPAST*-AAV9 n = 6, and *SPAST*-C448Y$^{+/-}$+*SPAST*-AAV9 n = 8. For statistical tests, one-way ANOVA with Tukey post hoc analysis was conducted. $^{*}p$ = 0.01 for *SPAST*-C448Y$^{+/-}$ non-inj: WT non-inj; $^{**}p$ = 0.001 for *SPAST*-C448Y$^{+/-}$ non-inj: WT+*SPAST*-AAV9; $^{***}p$ < 0.001 for *SPAST*-C448Y$^{+/-}$+*SPAST*-AAV9: *SPAST*-C448Y$^{+/-}$ non-inj. (D) Cross-sections of cervical and lumbar levels were used to investigate axonal degeneration of the dorsal column. The total axon number per ROI is quantified in the dorsal column of *SPAST*-C448Y$^{+/-}$ relative to WT. The quantifications show a reduced number of axon in *SPAST*-C448Y$^{+/-}$ non-inj. Each data point is an average of 8–12 randomly selected sections from 1 animal. For SMI311 staining, animal number n = 4, for all experimental groups. For statistical tests, one-way ANOVA with Tukey post hoc analysis was conducted. $^{*}p$ = 0.02 for *SPAST*-C448Y$^{+/-}$ non-inj: WT non-inj and for *SPAST*-C448Y$^{+/-}$ non-inj: WT+*SPAST*-AAV9. Scale bar, 50 µm.

after vector administration. We acknowledge that acute or subacute hepatic responses may have been missed, and future studies will include earlier and later time points to provide a more comprehensive safety profile. Incorporating such analyses will be particularly important for identifying any short-term effects related to vector delivery or SPAST silencing without replacement.

Based on the present results, it is unknown whether the silence or the replace component of the gene therapy is more crucial, or if they are both crucial. If the replace component is crucial, then it is unknown whether replacing M1 or replacing M87 is more important or if they are both important. While the strength of the present approach is that the therapy covers all of these possibilities, it may be that a better version of the therapy can be developed with more knowledge. For example, if replenishing the spastin levels beyond those provided by the healthy SPAST gene in the patients is not necessary, then the AAV9-based approach could be replaced with allele-specific antisense oligonucleotides that only curtail expression of the mutant gene.

What do our gene therapy results portend for the *SPG4*-HSP patient community? While the results with the mouse model are impressive, there are several challenges for human patients, not the least of which is being able to transduce enough neurons in the much larger human brain compared to the mouse brain. Another is the fact that a human patient may have a great deal of mutant M1 already accumulated in their CST, and this would not likely diminish very quickly just because the synthesis of more is halted. Finally, the CST may already be degenerated, even if the patient has not yet suffered serious symptoms, and silencing and replacing the mutant protein would not likely reverse that degeneration. These challenges are even more profound for patients who are already suffering from severe symptoms. Children may have better potential for restoration of function because their nervous system is still developing, but for most patients, the gene therapy approach on its own may be limited to preventing the symptoms from worsening rather than reversing them. In future studies, M1-specific protein degraders, such as intrabodies[72] derived from recombinant M1 antibodies, may offer a combinatorial or alternative approach to silencing SPAST gene expression, particularly in cases in which M1 mutant protein has already accumulated.

The best treatment for patients at all stages of the disease is probably combinatorial therapy, in which gene therapy is combined with other therapies to mitigate the toxicity of the mutant M1 already accumulated and therapies to stimulate the sprouting of healthy nerves to take the place of the lost connections. While the present study focuses on early pre-symptomatic intervention, we recognize that translating gene therapy into a feasible treatment for *SPG4*-HSP requires efficacy across various stages of disease progression. Given the absence of robust prenatal screening methods and validated early biomarkers, pre-symptomatic treatment may not be practical for many patients. Therefore, evaluating this therapeutic approach at symptomatic stages will be a critical next step. Our

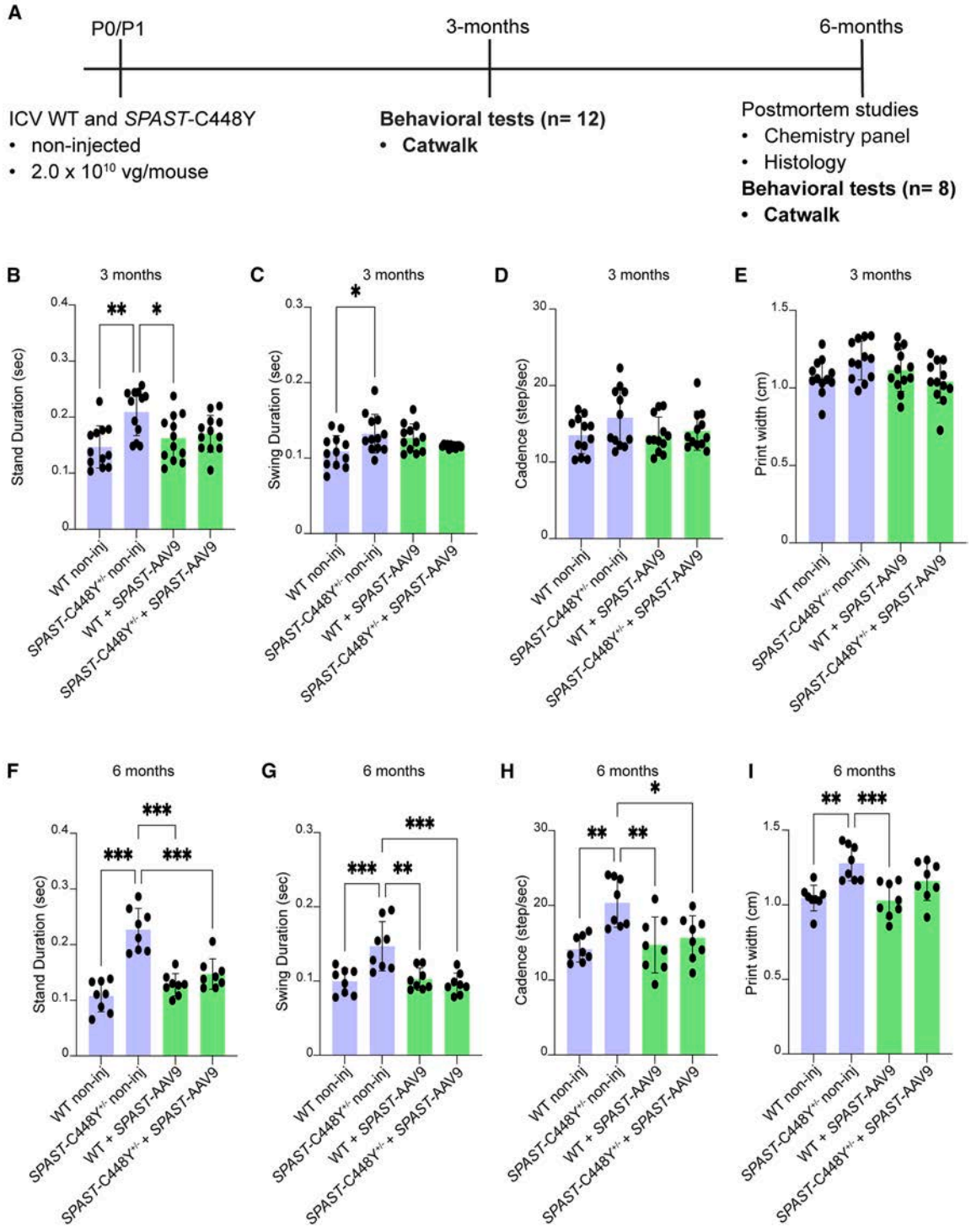

Figure 7. The *SPAST*-AAV9 treatment improves the gait impairment in *SPAST*-C448Y$^{+/-}$ mice

(A) Non-injected or 2.0 × 10^{10} vg/mouse of *SPAST*-AAV9 vector were administered ICV at P0/P1 to an equal number of males and females from WT and *SPAST*-C448Y$^{+/-}$ mice. At 3 and 6 months post-injection, mice were subjected to behavioral tests using CatWalk. (B–E) Parameters assessed at 3 months post-injection; where (B) stand and (C) swing durations are significantly increased in *SPAST*-C448Y$^{+/-}$ non-inj compared to WT non-inj, while no changes are detected among the groups for (D) cadence and (E) print width. Each data point represents a measurement from an individual animal, $n = 12$. Data are represented as mean ± SD. For statistical tests, one-way ANOVA with Tukey post hoc analysis was conducted. *$p = 0.03$ and **$p = 0.002$ in (B); *$p = 0.02$ in (C). (F–I) Gait parameters were also assessed at 6 months post-injection; (F) stand

(legend continued on next page)

Please cite this article in press as: Piermarini et al., Intracerebroventricular *SPAST*-AAV9 gene therapy prevents manifestation of symptoms in a mouse model of *SPG4* hereditary spastic paraplegia, Molecular Therapy (2025), https://doi.org/10.1016/j.ymthe.2025.11.029

long-term goal is to develop gene therapy not only as a preventive strategy but also as part of a comprehensive, multi-tiered therapeutic regimen that can restore lost function and provide benefit to patients regardless of when during disease progression the treatment is initiated. Providing effective therapeutics for all members of the *SPG4*-HSP patient community, regardless of disease progression status, is the larger goal of our research.

MATERIALS AND METHODS

Animals

All of the animal experiments were performed in compliance with the NIH's *Guide for the Care and Use of Laboratory Animals* and were reviewed and approved by the Institutional Animal Care and Use Committee (IACUC) at Drexel University. The animal work for this study was carried out under the project license 1045165, protocol number LA-23-004.

Colony generation, breeding strategy, and housing

The transgenic *SPAST*-C448Y mouse carries a point mutation in exon 11 of human full-length SPAST (SPAST c.1343g>a [p.Cys448-Tyr], NM_014946.3, CCDS_1778.1) inserted into the Gt26Sor locus to allow the expression of human SPAST to be dependent upon Cre recombinase. *SPAST*-C448Y$^{+/-}$ mice (human *SPAST*-C448Y heterozygous mice) were generated by mating a ubiquitous Cre mouse strain with the locked *SPAST*-C448Y mice as described by Qiang et al.[9] Next, we used a Het × Het paradigm to generate all of the mice used in this study, both WT and *SPAST*-C448Y$^{+/-}$. This breeding strategy allows us to collect all of the genotypes needed for the study from the litters. Mice (males or females) were group housed as 5 per cage under a 12-h light/dark cycle and divided into experimental groups: as non-injected or *SPAST*-AAV9 injected. Temperature and humidity were kept constant, and mice had free access to drinking water and food.

Genotyping PCR

Genomic DNA (gDNA) was isolated using the EZ Tissue DNA Isolation Kit (catalog no. M1003, EZ Bioresearch). At 21 days of age, mice were weened, and ear clipping (no larger than 2 mm) was used to mark them and to collect ear tissue for genotyping analysis. To determine zygosity in *SPAST*-C448Y mice, 40 ng gDNA was used to run a quantitative real-time PCR, using iTaq Universal SYBR Green Supermix (catalog no. 1725120, Bio-Rad). Quantitative real-time PCR is carried out with a pair of primers that are specific for the human spastin (forward: 5′-AGCACAACTTGCTAGAATGACTG-3′; reverse: 5′-AAGTTTGAGGGCTGACGCTG-3′), and mouse interleukin-2 (forward: 5′-CTAGGCCACAGAATTGAAAGATCT-3′; reverse: 5′-GTAGGTGGAAATTCTAGCATCATCC-3′) is used as a control gene to identify genotypes based on relative DNA content. The PCR reaction is carried out using the StepOne Real-Time PCR System (catalog no. 4376357, Applied Biosystems). Genotypes were detected using LinRegPCR software version 5.1.1.

ICV injections of the *SPAST*-AAV9 vector

All surgical procedures were performed under hypothermia in neonatal mice. P0/P1 littermates were temporarily separated from their mother and transported to the surgical suite for the injection of the *SPAST*-AAV9. Pups were deeply anesthetized by hypothermia on ice for 10–12 min, with no direct contact of the skin with the ice to avoid complications such as tissue damage. Following anesthesia, mice were positioned using stereotaxic coordinates to manually perform the ICV injection of the *SPAST*-AAV9 at a dosage of 2.0×10^{10} vg/mouse, for a total of 2 μL each ventricle using a 10-μL Hamilton RN (removable needle) syringe (catalog no. 80330, Hamilton) with a 32G needle (catalog no. 7803-04, Hamilton). We selected a 2 μL injection volume based on published neonatal ICV protocols in P0 mouse pups.[73–75] The needle was held perpendicular to the skull during the insertion, and the *SPAST*-AAV9 was administered slowly over 1 min per hemisphere into the lateral ventricle at approximately 1 mm lateral and 1 mm posterior to bregma at a depth of 2 mm. Manual ICV injections were carried out under a stereomicroscope, with the pups positioned in a custom neonatal mold and gently restrained by hand, while maintained under hypothermia-induced anesthesia on ice. Following the injection, pups were placed on a warming pad until fully recovered before being returned to the dam. At P21, animals were weaned and separated according to their sex until they were of the appropriate age to assess gait alterations.

M1-specific antibody generation

Standard procedures were applied by GeneScript for the production and affinity purification of rabbit polyclonal antibodies to M1, using the first 28 aa of M1 as the antigen.

WB analysis of spastin isoform expression in mouse tissues

Four animals per group (2 males and 2 females) were used for the analyses. CNS (brain and spinal cord) and peripheral tissues (liver, 2 males and 1 females) from WT and *SPAST*-C448Y$^{+/-}$ were collected at 6 months of age and via euthanasia by intraperitoneal injection of pentobarbital sodium and phenytoin sodium solution (Euthasol 150 mg/kg; catalog no. 50989056912, VEDCO). Dissected tissues were homogenized in ice-cold 1× radioimmunoprecipitation assay buffer (1X RIPA buffer, catalog no. 89901, Thermo Fisher) in the presence of a phosphatase/protease inhibitor cocktail (catalog nos. A32953 and A32957 for protease and phosphatase inhibitors, respectively, Pierce). Tissue lysates, 50 μg, were electrophoresed on 12% Bis/Tris gels (catalog no. 456-1084, Bio-Rad) to perform SDS-PAGE. Proteins were then transferred to a polyvinylidene fluoride membrane (PVDF, catalog no. 1620177, Bio-Rad), blocked with Intercept TBS Blocking Buffer (catalog no. 927-60001, Li-Cor) for

duration, (G) swing duration, (H) cadence, and (I) print widths are worsened in *SPAST*-C448Y$^{+/-}$ non-inj compared to WT non-inj. Each data point represents a measurement from an individual animal, $n = 8$. Data are represented as mean ± SD. For statistical tests, one-way ANOVA with Tukey post hoc analysis was conducted. ***$p < 0.001$ in (F); **$p = 0.002$ and ***$p < 0.001$ in (G); *$p = 0.02$ and **$p = 0.002$ for *SPAST*-C448Y$^{+/-}$ non-inj: WT non-inj, **$p = 0.004$ for *SPAST*-C448Y$^{+/-}$ non-inj: WT+*SPAST*-AAV9 in (H); **$p = 0.002$ and ***$p < 0.001$ in (I).

2 h at room temperature (RT). Primary antibodies for M1-specific (1:200), general spastin (1:200, Abcam catalog no. ab77144), and glyceraldehyde 3-phosphate dehydrogenase (GAPDH) (1:10,000, Abcam, catalog no. AB8245) were diluted in TBS (Tris-buffered saline) Blocking Buffer and incubated overnight at 4°C. After rinsing with TBS 1× + 0.25% Tween 20 (TBS-T 1×) 3 times per 10 min at RT, membranes were incubated with IRDye Infrared Dye secondary antibodies 1:5,000 (Li-Cor) at RT for 2 h protected from light, and proteins were visualized using the Odyssey CLx Imaging System (Li-Cor).

Analyses were performed by evaluating the band intensities using Image Studio software version 5.2.5 provided by Li-Cor. The levels of M1 and M87 were calculated as ratios to the level of GAPDH in the same sample. Ratios in WT animals were taken as 1, and the ratios in *SPAST*-C448Y$^{+/-}$ were presented relative to those in the WT animals ± SD.

Serum collection and preparation for blood chemistry panel

To collect the sera, animals were sacrificed using CO_2 for approximately 5 min, and the thoracic cavity was carefully opened to expose the heart. Heart puncture at the right atrium was then performed to collect the blood from the thoracic cavity using a 0.5-M EDTA, pH 8 coated syringe into a BD Vacutainer serum tube (catalog no. BD366668). To separate the clot from serum, the tube was then spun at 3,000 × *g* for 10 min at 4°C in a swing basket centrifuge, and the serum (supernatant) was transferred into a new tube and stored at −80°C until the analyses. The sera were shipped to the University of Michigan Unit for Laboratory Animal Medicine Pathology Core facility to run a full chemistry panel, which includes AST, ALT, T.Bil, albumin, CREA, T.Pro, and electrolytes (Na, K, Cl). Because the syringes were coated with EDTA, creatine kinase and blood urea nitrogen values were not considered, while the ALT results have been multiplied by a factor of 1.02 as suggested by the facility to reflect the serum levels of ALT.

Tissue collection and preparation for anatomical analyses

A total of 6–8 animals per group were considered for the anatomical analyses. WT and *SPAST*-C448Y$^{+/-}$ were collected at 6 months of age and sacrificed by intraperitoneal injection of Euthasol solution at a dose of 150 mg/kg. Transcardial perfusion was performed by using 0.9% NaCl (catalog no. BP358-212, Fisher Bioreagent) to rinse out blood, followed by 4% paraformaldehyde (PFA, catalog no. 19202, Electron Microscopy Sciences) in 0.1 M phosphate buffer for tissue fixation. CNS tissues (brain and spinal cord) were dissected out and post-fixed overnight in 4% PFA, followed by sequential immersion in 15% and 30% sucrose (catalog no. 1310, Fisher Bioreagent) before embedding into M1 embedding media (catalog no. 1310, Thermo Scientific). We obtained 40-μm cross-sections from the cervical and lumbar levels of the spinal cord to assess axonal degeneration using antibodies SMI311 and SMI312 against total or phospho-neurofilaments, respectively. Sections were subjected to a quenching step for 2 h at RT to reduce the reaction of endogenous peroxidases, followed by a blocking step in 10% goat serum with 0.1% Triton X-100. Cross-sections of the spinal cord were then stained for the neurofilament markers.

SMI311 (1:500, BioLegend, catalog no. 837801) or SMI312 (1:500, BioLegend, catalog no. 837904) were diluted in PBS 1× overnight at 4°C, followed by incubation with Alexa Fluor 488-conjugated secondary antibody (1:1,000; catalog no. A11029, Life Technologies) for 2 h at RT. Glass coverslips were mounted on microscope slides with Fluoro-Gel (catalog no. 17985-10, Electron Microscopy Sciences) to reduce fading of fluorescence, and samples were examined by a Leica TCS SP8 confocal microscope using a 63× oil immersion objective. Z stacks were collected with a step size of 0.3 μm over a total depth of about 10 μm. Quantifications were performed on maximum intensity projections generated from the entire z stack using ImageJ/Fiji. Acquisition parameters were kept constant across all samples. Specifically, SMI311 quantification was performed by counting the number of SMI311^{+} axons in the dorsal column at both cervical and lumbar levels. For SMI312, fluorescence intensity was evaluated at the lumbar level in the dorsal column by measuring the corrected total fluorescence intensity, calculated as the total fluorescent signal within a defined region of interest minus background fluorescence. Both analyses were performed using ImageJ software version 2.9.0/1.53t.

Behavioral assay: CatWalk analyses

The CatWalk assay was used to measure gait abnormalities associated with CST degeneration. The Noldus CatWalk XT automated gait analysis system consists of a black glass platform of 1.3 m above a high-resolution video camera, and it is located in a dark and silent room. A green light-emitting diode fluorescent light is reflected through the glass platform, wherever the mouse makes contact along the platform, the green light is scattered, and the camera underneath acquires and transforms each scene into a digital image. The CatWalk station is also equipped with software that enables the analysis of the videos and produces a large amount of data related to more than 90 different parameters of gait, such as speed, timing, and coordination. Mice were transported to an isolated behavior room 30 min before testing for acclimation. Each mouse enrolled in the project underwent 1 week of training and 1 week of recording for gait parameters analysis as previously described with modifications.[10] Before recording, animals were individually placed on the CatWalk and allowed to move freely in both directions. For detection of all parameters used in the experiments, the camera gain was set to 20 dB and the detection threshold to 0.10. All runs with a duration between 0.50 and 5.00 s to complete the walkway and a maximum speed variation of 60% were considered successful runs. A compliant run is described as a mouse walking across the runway without stopping, turning around, or changing direction. For each animal at each time point a minimum of three compliant runs was used for analyses. Compliant runs were classified for all limbs and statistically analyzed. Given that HSP patients display slow walking speed,[68] the gait analysis for all the groups was made by selecting only animals for which walking speed will range in the average speed ± SD of *SPAST*-C448Y$^{+/-}$ non-inj mice. WT and *SPAST*-C448Y$^{+/-}$ from all the experimental groups were subjected to behavioral testing at 3 and 6 months of age.

In the present study, parameters that correlate with gait deficiencies of HSP patients were chosen for the analysis.[68] The gait of the animals was evaluated by the following 4 different parameters. The stand duration (or stand phase) is expressed in seconds and represents the time in which a paw is in contact with the glass plate; the swing duration is also expressed in seconds and represents the time in which the paw is not in contact with the walkway; the cadence represents the frequency of steps the mouse takes during the trial and it is measured in steps per second; and the step width or print width is the width (vertical direction) of the complete paw print.

Graphs and statistics

All of the statistical analyses were performed and graphs prepared using GraphPad Prism version 10.4.0. Group differences were assessed using a one-way analysis of variance (ANOVA), followed by Tukey's post hoc test. Significance was defined as $^{*}p < 0.05$, using the following annotations: $^{*}p < 0.05$, $^{**}p < 0.002$, and $^{***}p < 0.001$ were considered statistically significant. Statistical significance and the number of samples are noted in the figure legends where appropriate. Schematics were created in BioRender (https://BioRender.com) with modifications.

DATA AND CODE AVAILABILITY

All data will be made available upon reasonable request to the corresponding authors.

ACKNOWLEDGMENTS

We acknowledge the assistance in this work of Koray Kirimtay for the M1 antibody testing and Angela Altadonna, Kendra Case, Skandha Ramakrishan, Neha Mohan, and Sean Vansen (all from Drexel University) for helping with the sera and tissues collection. This work is supported by separate grants from the Spastic Paraplegia Foundation to E.P., P.W.B., and L.Q., and from the NIH (National Institute of Neurological Disorders and Stroke) to P.W.B. (R01 NS118177) and L.Q. (R01 NS115977). Generous additional funding and ongoing support at all levels were provided by the Cure *SPG4* Foundation, The Lilly and Blair Foundation, *SPG4* Cure for Jack Laidlaw, and the Maurya Koduri Foundation. This work is dedicated to the children living with *SPG4* Hereditary Spastic Paraplegia and the limitless dedication of their parents to find a cure. The authors reserve the right to intellectual properties related to future commercialization of the vector or a modification of it for future clinical trials on patients.

AUTHOR CONTRIBUTIONS

The project was conceived collaboratively by P.W.B., M.S.-E., and E.P. E.P. designed and performed all of the experiments, analyzed the data, performed the statistical analyses, and prepared the figures. The vector was generated and validated by M.S.-E. S.G. and E.P. performed the ICV injections, and together they analyzed the histology. Technical input for the vector design was also provided by L.Q. and H.G.-E. The first draft of the manuscript was written by E.P. and P.W.B. All the authors read, revised, and approved the manuscript.

DECLARATION OF INTERESTS

The authors declare no competing interests.

REFERENCES

1. Blackstone, C. (2018). Converging cellular themes for the hereditary spastic paraplegias. Curr. Opin. Neurobiol. *51*, 139–146. https://doi.org/10.1016/j.conb.2018.04.025.

2. Blackstone, C., O'Kane, C.J., and Reid, E. (2011). Hereditary spastic paraplegias: membrane traffic and the motor pathway. Nat. Rev. Neurosci. *12*, 31–42. https://doi.org/10.1038/nrn2946.

3. Wang, X.C., Liu, R.H., Wang, T., Wang, Y., Jiang, Y., Chen, D.D., Wang, X.Y., Hou, T.S., and Kong, Q.X. (2023). A novel missense mutation in SPAST causes hereditary spastic paraplegia in male members of a family: A case report. Mol. Med. Rep. *27*, 79. https://doi.org/10.3892/mmr.2023.12966.

4. McDermott, C., White, K., Bushby, K., and Shaw, P. (2000). Hereditary spastic paraparesis: a review of new developments. J. Neurol. Neurosurg. Psychiatry *69*, 150–160. https://doi.org/10.1136/jnnp.69.2.150.

5. Hazan, J., Fonknechten, N., Mavel, D., Paternotte, C., Samson, D., Artiguenave, F., Davoine, C.S., Cruaud, C., Dürr, A., Wincker, P., et al. (1999). Spastin, a new AAA protein, is altered in the most frequent form of autosomal dominant spastic paraplegia. Nat. Genet. *23*, 296–303. https://doi.org/10.1038/15472.

6. Leo, L., Weissmann, C., Burns, M., Kang, M., Song, Y., Qiang, L., Brady, S.T., Baas, P.W., and Morfini, G. (2017). Mutant spastin proteins promote deficits in axonal transport through an isoform-specific mechanism involving casein kinase 2 activation. Hum. Mol. Genet. *26*, 2321–2334. https://doi.org/10.1093/hmg/ddx125.

7. Solowska, J.M., D'Rozario, M., Jean, D.C., Davidson, M.W., Marenda, D.R., and Baas, P.W. (2014). Pathogenic mutation of spastin has gain-of-function effects on microtubule dynamics. J. Neurosci. *34*, 1856–1867. https://doi.org/10.1523/JNEUROSCI.3309-13.2014.

8. Solowska, J.M., Rao, A.N., and Baas, P.W. (2017). Truncating mutations of SPAST associated with hereditary spastic paraplegia indicate greater accumulation and toxicity of the M1 isoform of spastin. Mol. Biol. Cell *28*, 1728–1737. https://doi.org/10.1091/mbc.E17-01-0047.

9. Qiang, L., Piermarini, E., Muralidharan, H., Yu, W., Leo, L., Hennessy, L.E., Fernandes, S., Connors, T., Yates, P.L., Swift, M., et al. (2019). Hereditary spastic paraplegia: gain-of-function mechanisms revealed by new transgenic mouse. Hum. Mol. Genet. *28*, 1136–1152. https://doi.org/10.1093/hmg/ddy419.

10. Piermarini, E., Akarsu, S., Connors, T., Kneussel, M., Lane, M.A., Morfini, G., Karabay, A., Baas, P.W., and Qiang, L. (2022). Modeling gain-of-function and loss-of-function components of SPAST-based hereditary spastic paraplegia using transgenic mice. Hum. Mol. Genet. *31*, 1844–1859. https://doi.org/10.1093/hmg/ddab367.

11. Denton, K.R., Lei, L., Grenier, J., Rodionov, V., Blackstone, C., and Li, X.J. (2014). Loss of spastin function results in disease-specific axonal defects in human pluripotent stem cell-based models of hereditary spastic paraplegia. Stem Cells *32*, 414–423. https://doi.org/10.1002/stem.1569.

12. Tadepalle, N., Robers, L., Veronese, M., Zentis, P., Babatz, F., Brodesser, S., Gruszczyk, A.V., Schauss, A., Höning, S., and Rugarli, E.I. (2020). Microtubule-dependent and independent roles of spastin in lipid droplet dispersion and biogenesis. Life Sci. Alliance *3*, e202000715. https://doi.org/10.26508/lsa.202000715.

13. Kumar, S.R., Markusic, D.M., Biswas, M., High, K.A., and Herzog, R.W. (2016). Clinical development of gene therapy: results and lessons from recent successes. Mol. Ther. Methods Clin. Dev. *3*, 16034. https://doi.org/10.1038/mtm.2016.34.

14. Liu, F., Li, R., Zhu, Z., Yang, Y., and Lu, F. (2024). Current developments of gene therapy in human diseases. MedComm *5*, e645. https://doi.org/10.1002/mco2.645.

15. Naldini, L. (2015). Gene therapy returns to centre stage. Nature *526*, 351–360. https://doi.org/10.1038/nature15818.

16. Keeler, A.M., Sapp, E., Chase, K., Sottosanti, E., Danielson, E., Pfister, E., Stoica, L., DiFiglia, M., Aronin, N., and Sena-Esteves, M. (2016). Cellular Analysis of Silencing the Huntington's Disease Gene Using AAV9 Mediated Delivery of Artificial Micro RNA into the Striatum of Q140/Q140 Mice. J. Huntingtons Dis. *5*, 239–248. https://doi.org/10.3233/JHD-160215.

17. Mendell, J.R., Al-Zaidy, S., Shell, R., Arnold, W.D., Rodino-Klapac, L.R., Prior, T.W., Lowes, L., Alfano, L., Berry, K., Church, K., et al. (2017). Single-Dose Gene-Replacement Therapy for Spinal Muscular Atrophy. N. Engl. J. Med. *377*, 1713–1722. https://doi.org/10.1056/NEJMoa1706198.

18. Saraiva, J., Nobre, R.J., and Pereira de Almeida, L. (2016). Gene therapy for the CNS using AAVs: The impact of systemic delivery by AAV9. J. Control Release *241*, 94–109. https://doi.org/10.1016/j.jconrel.2016.09.011.

19. Vance, M., Llanga, T., Bennett, W., Woodard, K., Murlidharan, G., Chungfat, N., Asokan, A., Gilger, B., Kurtzberg, J., Samulski, R.J., and Hirsch, M.L. (2016). AAV Gene Therapy for MPS1-associated Corneal Blindness. Sci. Rep. *6*, 22131. https://doi.org/10.1038/srep22131.

20. Belur, L.R., Romero, M., Lee, J., Podetz-Pedersen, K.M., Nan, Z., Riedl, M.S., Vulchanova, L., Kitto, K.F., Fairbanks, C.A., Kozarsky, K.F., et al. (2021). Comparative Effectiveness of Intracerebroventricular, Intrathecal, and Intranasal Routes of AAV9 Vector Administration for Genetic Therapy of Neurologic Disease in Murine Mucopolysaccharidosis Type I. Front. Mol. Neurosci. *14*, 618360. https://doi.org/10.3389/fnmol.2021.618360.

21. Kota, J., Chivukula, R.R., O'Donnell, K.A., Wentzel, E.A., Montgomery, C.L., Hwang, H.W., Chang, T.C., Vivekanandan, P., Torbenson, M., Clark, K.R., et al. (2009). Therapeutic microRNA delivery suppresses tumorigenesis in a murine liver cancer model. Cell *137*, 1005–1017. https://doi.org/10.1016/j.cell.2009.04.021.

22. Miyazaki, Y., Adachi, H., Katsuno, M., Minamiyama, M., Jiang, Y.M., Huang, Z., Doi, H., Matsumoto, S., Kondo, N., Iida, M., et al. (2012). Viral delivery of miR-196a ameliorates the SBMA phenotype via the silencing of CELF2. Nat. Med. *18*, 1136–1141. https://doi.org/10.1038/nm.2791.

23. Stoica, L., Todeasa, S.H., Cabrera, G.T., Salameh, J.S., ElMallah, M.K., Mueller, C., Brown, R.H., Jr., and Sena-Esteves, M. (2016). Adeno-associated virus-delivered artificial microRNA extends survival and delays paralysis in an amyotrophic lateral sclerosis mouse model. Ann. Neurol. *79*, 687–700. https://doi.org/10.1002/ana.24618.

24. Xia, H., Mao, Q., Eliason, S.L., Harper, S.Q., Martins, I.H., Orr, H.T., Paulson, H.L., Yang, L., Kotin, R.M., and Davidson, B.L. (2004). RNAi suppresses polyglutamine-induced neurodegeneration in a model of spinocerebellar ataxia. Nat. Med. *10*, 816–820. https://doi.org/10.1038/nm1076.

25. Leone, P., Shera, D., McPhee, S.W.J., Francis, J.S., Kolodny, E.H., Bilaniuk, L.T., Wang, D.J., Assadi, M., Goldfarb, O., Goldman, H.W., et al. (2012). Long-term follow-up after gene therapy for canavan disease. Sci. Transl. Med. *4*, 165ra163. https://doi.org/10.1126/scitranslmed.3003454.

26. Broekman, M.L.D., Tierney, L.A., Benn, C., Chawla, P., Cha, J.H., and Sena-Esteves, M. (2009). Mechanisms of distribution of mouse beta-galactosidase in the adult GM1-gangliosidosis brain. Gene Ther. *16*, 303–308. https://doi.org/10.1038/gt.2008.149.

27. Lin, D., Fantz, C.R., Levy, B., Rafi, M.A., Vogler, C., Wenger, D.A., and Sands, M.S. (2005). AAV2/5 vector expressing galactocerebrosidase ameliorates CNS disease in the murine model of globoid-cell leukodystrophy more efficiently than AAV2. Mol. Ther. *12*, 422–430. https://doi.org/10.1016/j.ymthe.2005.04.019.

28. Macauley, S.L., Wong, A.M.S., Shyng, C., Augner, D.P., Dearborn, J.T., Pearse, Y., Roberts, M.S., Fowler, S.C., Cooper, J.D., Watterson, D.M., and Sands, M.S. (2014). An anti-neuroinflammatory that targets dysregulated glia enhances the efficacy of CNS-directed gene therapy in murine infantile neuronal ceroid lipofuscinosis. J. Neurosci. *34*, 13077–13082. https://doi.org/10.1523/JNEUROSCI.2518-14.2014.

29. Rafi, M.A., Zhi Rao, H., Passini, M.A., Curtis, M., Vanier, M.T., Zaka, M., Luzi, P., Wolfe, J.H., and Wenger, D.A. (2005). AAV-mediated expression of galactocerebrosidase in brain results in attenuated symptoms and extended life span in murine models of globoid cell leukodystrophy. Mol. Ther. *11*, 734–744. https://doi.org/10.1016/j.ymthe.2004.12.020.

30. Spampanato, C., De Leonibus, E., Dama, P., Gargiulo, A., Fraldi, A., Sorrentino, N.C., Russo, F., Nusco, E., Auricchio, A., Surace, E.M., and Ballabio, A. (2011). Efficacy of a combined intracerebral and systemic gene delivery approach for the treatment of a severe lysosomal storage disorder. Mol. Ther. *19*, 860–869. https://doi.org/10.1038/mt.2010.299.

31. Wolf, D.A., Lenander, A.W., Nan, Z., Belur, L.R., Whitley, C.B., Gupta, P., Low, W.C., and McIvor, R.S. (2011). Direct gene transfer to the CNS prevents emergence of neurologic disease in a murine model of mucopolysaccharidosis type I. Neurobiol. Dis. *43*, 123–133. https://doi.org/10.1016/j.nbd.2011.02.015.

32. Hordeaux, J., Hinderer, C., Buza, E.L., Louboutin, J.P., Jahan, T., Bell, P., Chichester, J.A., Tarantal, A.F., and Wilson, J.M. (2019). Safe and Sustained Expression of Human Iduronidase After Intrathecal Administration of Adeno-Associated Virus Serotype 9 in Infant Rhesus Monkeys. Hum. Gene Ther. *30*, 957–966. https://doi.org/10.1089/hum.2019.012.

33. Hordeaux, J., Hinderer, C., Goode, T., Katz, N., Buza, E.L., Bell, P., Calcedo, R., Richman, L.K., and Wilson, J.M. (2018). Toxicology Study of Intra-Cisterna Magna Adeno-Associated Virus 9 Expressing Human Alpha-L-Iduronidase in Rhesus Macaques. Mol. Ther. Methods Clin. Dev. *10*, 79–88. https://doi.org/10.1016/j.omtm.2018.06.003.

34. Watson, G., Bastacky, J., Belichenko, P., Buddhikot, M., Jungles, S., Vellard, M., Mobley, W.C., and Kakkis, E. (2006). Intrathecal administration of AAV vectors for the treatment of lysosomal storage in the brains of MPS I mice. Gene Ther. *13*, 917–925. https://doi.org/10.1038/sj.gt.3302735.

35. Belur, L.R., Podetz-Pedersen, K.M., Tran, T.A., Mesick, J.A., Singh, N.M., Riedl, M., Vulchanova, L., Kozarsky, K.F., and McIvor, R.S. (2020). Intravenous delivery for treatment of mucopolysaccharidosis type I: A comparison of AAV serotypes 9 and rh10. Mol. Genet. Metab. Rep. *24*, 100604. https://doi.org/10.1016/j.ymgmr.2020.100604.

36. Hinderer, C., Bell, P., Gurda, B.L., Wang, Q., Louboutin, J.P., Zhu, Y., Bagel, J., O'Donnell, P., Sikora, T., Ruane, T., et al. (2014). Liver-directed gene therapy corrects cardiovascular lesions in feline mucopolysaccharidosis type I. Proc. Natl. Acad. Sci. USA *111*, 14894–14899. https://doi.org/10.1073/pnas.1413645111.

37. Mancuso, G., and Rugarli, E.I. (2008). A cryptic promoter in the first exon of the SPG4 gene directs the synthesis of the 60-kDa spastin isoform. BMC Biol. *6*, 31. https://doi.org/10.1186/1741-7007-6-31.

38. Ramakrishnan, S., Mohan, N., Dong, Z., Liu, M., and Qiang, L. (2025). Unraveling Isoform Complexity: The Roles of M1- and M87-Spastin in Spastic Paraplegia 4 (SPG4). Mov. Disord. *40*, 420–430. https://doi.org/10.1002/mds.30072.

39. Kuo, Y.W., Trottier, O., Mahamdeh, M., and Howard, J. (2019). Spastin is a dual-function enzyme that severs microtubules and promotes their regrowth to increase the number and mass of microtubules. Proc. Natl. Acad. Sci. USA *116*, 5533–5541. https://doi.org/10.1073/pnas.1818824116.

40. Sakoe, K., Shioda, N., and Matsuura, T. (2021). A newly identified NES sequence present in spastin regulates its subcellular localization and microtubule severing activity. Biochim. Biophys. Acta Mol. Cell Res. *1868*, 118862. https://doi.org/10.1016/j.bbamcr.2020.118862.

41. Mohan, N., Qiang, L., Morfini, G., and Baas, P.W. (2021). Therapeutic Strategies for Mutant SPAST-Based Hereditary Spastic Paraplegia. Brain Sci. *11*, 1081. https://doi.org/10.3390/brainsci11081081.

42. Plaud, C., Joshi, V., Kajevu, N., Poüs, C., Curmi, P.A., and Burgo, A. (2018). Functional differences of short and long isoforms of spastin harboring missense mutation. Dis. Model. Mech. *11*, dmm033704. https://doi.org/10.1242/dmm.033704.

43. Solowska, J.M., Garbern, J.Y., and Baas, P.W. (2010). Evaluation of loss of function as an explanation for SPG4-based hereditary spastic paraplegia. Hum. Mol. Genet. *19*, 2767–2779. https://doi.org/10.1093/hmg/ddq177.

44. Arribat, Y., Grepper, D., Lagarrigue, S., Qi, T., Cohen, S., and Amati, F. (2020). Spastin mutations impair coordination between lipid droplet dispersion and reticulum. PLoS Genet. *16*, e1008665. https://doi.org/10.1371/journal.pgen.1008665.

45. Liu, Q., Zhang, G., Ji, Z., and Lin, H. (2021). Molecular and cellular mechanisms of spastin in neural development and disease (Review). Int. J. Mol. Med. *48*, 218. https://doi.org/10.3892/ijmm.2021.5051.

46. Lumb, J.H., Connell, J.W., Allison, R., and Reid, E. (2012). The AAA ATPase spastin links microtubule severing to membrane modelling. Biochim. Biophys. Acta *1823*, 192–197. https://doi.org/10.1016/j.bbamcr.2011.08.010.

47. Rizo, T., Gebhardt, L., Riedlberger, J., Eberhardt, E., Fester, L., Alansary, D., Winkler, J., Turan, S., Arnold, P., Niemeyer, B.A., et al. (2022). Store-operated calcium entry is reduced in spastin-linked hereditary spastic paraplegia. Brain. *145*, 3131–3146. https://doi.org/10.1093/brain/awac122.

48. Deluca, G.C., Ebers, G.C., and Esiri, M.M. (2004). The extent of axonal loss in the long tracts in hereditary spastic paraplegia. Neuropathol. Appl. Neurobiol. *30*, 576–584. https://doi.org/10.1111/j.1365-2990.2004.00587.x.

49. Solowska, J.M., Morfini, G., Falnikar, A., Himes, B.T., Brady, S.T., Huang, D., and Baas, P.W. (2008). Quantitative and functional analyses of spastin in the nervous system: implications for hereditary spastic paraplegia. J. Neurosci. *28*, 2147–2157. https://doi.org/10.1523/JNEUROSCI.3159-07.2008.

50. Chen, R., Du, S., Yao, Y., Zhang, L., Luo, J., Shen, Y., Xu, Z., Zeng, X., Zhang, L., Liu, M., et al. (2022). A Novel SPAST Mutation Results in Spastin Accumulation and Defects in Microtubule Dynamics. Mov. Disord. *37*, 598–607. https://doi.org/10.1002/mds.28885.

51. Ji, Z.S., Li, J.P., Fu, C.H., Luo, J.X., Yang, H., Zhang, G.W., Wu, W., and Lin, H.S. (2021). Spastin interacts with collapsin response mediator protein 3 to regulate neurite growth and branching. Neural Regen. Res. *16*, 2549–2556. https://doi.org/10.4103/1673-5374.313052.

52. Salinas, S., Carazo-Salas, R.E., Proukakis, C., Cooper, J.M., Weston, A.E., Schiavo, G., and Warner, T.T. (2005). Human spastin has multiple microtubule-related functions. J. Neurochem. *95*, 1411–1420. https://doi.org/10.1111/j.1471-4159.2005.03472.x.

53. Gray, S.J., Foti, S.B., Schwartz, J.W., Bachaboina, L., Taylor-Blake, B., Coleman, J., Ehlers, M.D., Zylka, M.J., McCown, T.J., and Samulski, R.J. (2011). Optimizing promoters for recombinant adeno-associated virus-mediated gene expression in the peripheral and central nervous system using self-complementary vectors. Hum. Gene Ther. *22*, 1143–1153. https://doi.org/10.1089/hum.2010.245.

54. Gadalla, K.K.E., Vudhironarit, T., Hector, R.D., Sinnett, S., Bahey, N.G., Bailey, M.E.S., Gray, S.J., and Cobb, S.R. (2017). Development of a Novel AAV Gene Therapy Cassette with Improved Safety Features and Efficacy in a Mouse Model of Rett Syndrome. Mol. Ther. Methods Clin. Dev. *5*, 180–190. https://doi.org/10.1016/j.omtm.2017.04.007.

55. Powers, S., Likhite, S., Gadalla, K.K., Miranda, C.J., Huffenberger, A.J., Dennys, C., Foust, K.D., Morales, P., Pierson, C.R., Rinaldi, F., et al. (2023). Novel MECP2 gene therapy is effective in a multicenter study using two mouse models of Rett syndrome and is safe in non-human primates. Mol. Ther. *31*, 2767–2782. https://doi.org/10.1016/j.ymthe.2023.07.013.

56. Cohen-Pfeffer, J.L., Gururangan, S., Lester, T., Lim, D.A., Shaywitz, A.J., Westphal, M., and Slavc, I. (2017). Intracerebroventricular Delivery as a Safe, Long-Term Route of Drug Administration. Pediatr. Neurol. *67*, 23–35. https://doi.org/10.1016/j.pediatrneurol.2016.10.022.

57. Cook, A.M., Mieure, K.D., Owen, R.D., Pesaturo, A.B., and Hatton, J. (2009). Intracerebroventricular administration of drugs. Pharmacotherapy *29*, 832–845. https://doi.org/10.1592/phco.29.7.832.

58. Lopes, A.T., Hausrat, T.J., Heisler, F.F., Gromova, K.V., Lombino, F.L., Fischer, T., Ruschkies, L., Breiden, P., Thies, E., Hermans-Borgmeyer, I., et al. (2020). Spastin depletion increases tubulin polyglutamylation and impairs kinesin-mediated neuronal transport, leading to working and associative memory deficits. PLoS Biol. *18*, e3000820. https://doi.org/10.1371/journal.pbio.3000820.

59. Keppler, A., Gretz, N., Schmidt, R., Kloetzer, H.M., Groene, H.J., Lelongt, B., Meyer, M., Sadick, M., and Pill, J. (2007). Plasma creatinine determination in mice and rats: an enzymatic method compares favorably with a high-performance liquid chromatography assay. Kidney Int. *71*, 74–78. https://doi.org/10.1038/sj.ki.5001988.

60. Meneton, P., Ichikawa, I., Inagami, T., and Schnermann, J. (2000). Renal physiology of the mouse. Am. J. Physiol. Ren. Physiol. *278*, F339–F351. https://doi.org/10.1152/ajprenal.2000.278.3.F339.

61. Moreno-Lopez, Y., Bichara, C., Delbecq, G., Isope, P., and Cordero-Erausquin, M. (2021). The corticospinal tract primarily modulates sensory inputs in the mouse lumbar cord. Elife *10*, e65304. https://doi.org/10.7554/eLife.65304.

62. Steward, O., Zheng, B., Ho, C., Anderson, K., and Tessier-Lavigne, M. (2004). The dorsolateral corticospinal tract in mice: an alternative route for corticospinal input to caudal segments following dorsal column lesions. J. Comp. Neurol. *472*, 463–477. https://doi.org/10.1002/cne.20090.

63. Dale, J.M., and Garcia, M.L. (2012). Neurofilament Phosphorylation during Development and Disease: Which Came First, the Phosphorylation or the Accumulation? J. Amino Acids *2012*, 382107. https://doi.org/10.1155/2012/382107.

64. Nagaraja, T.N., Gourie-Devi, M., Nalini, A., and Raju, T.R. (1994). Neurofilament phosphorylation is enhanced in cultured chick spinal cord neurons exposed to cerebrospinal fluid from amyotrophic lateral sclerosis patients. Acta Neuropathol. *88*, 349–352. https://doi.org/10.1007/BF00310378.

65. K, S.V.A., Dissanayake, D., Gunatilake, M., Kuzhandai Velu, V., and Paranthaman, M. (2023). A short review on behavioural assessment methods in rodents. Bioinformation *19*, 866–870. https://doi.org/10.6026/97320630019866.

66. Ruan, J., and Yao, Y. (2020). Behavioral tests in rodent models of stroke. Brain Hemorrhages *1*, 171–184. https://doi.org/10.1016/j.hest.2020.09.001.

67. Pitzer, C., Kurpiers, B., and Eltokhi, A. (2021). Gait performance of adolescent mice assessed by the CatWalk XT depends on age, strain and sex and correlates with speed and body weight. Sci. Rep. *11*, 21372. https://doi.org/10.1038/s41598-021-00625-8.

68. Serrao, M., Rinaldi, M., Ranavolo, A., Lacquaniti, F., Martino, G., Leonardi, L., Conte, C., Varrecchia, T., Draicchio, F., Coppola, G., et al. (2016). Gait Patterns in Patients with Hereditary Spastic Paraparesis. PLoS One *11*, e0164623. https://doi.org/10.1371/journal.pone.0164623.

69. Julien, C., Lissouba, A., Madabattula, S., Fardghassemi, Y., Rosenfelt, C., Androschuk, A., Strautman, J., Wong, C., Bysice, A., O'Sullivan, J., et al. (2016). Conserved pharmacological rescue of hereditary spastic paraplegia-related phenotypes across model organisms. Hum. Mol. Genet. *25*, 1088–1099. https://doi.org/10.1093/hmg/ddv632.

70. Orso, G., Martinuzzi, A., Rossetto, M.G., Sartori, E., Feany, M., and Daga, A. (2005). Disease-related phenotypes in a Drosophila model of hereditary spastic paraplegia are ameliorated by treatment with vinblastine. J. Clin. Invest. *115*, 3026–3034. https://doi.org/10.1172/JCI24694.

71. Sherwood, N.T., Sun, Q., Xue, M., Zhang, B., and Zinn, K. (2004). Drosophila spastin regulates synaptic microtubule networks and is required for normal motor function. PLoS Biol. *2*, e429. https://doi.org/10.1371/journal.pbio.0020429.

72. Messer, A., and Butler, D.C. (2020). Optimizing intracellular antibodies (intrabodies/nanobodies) to treat neurodegenerative disorders. Neurobiol. Dis. *134*, 104619. https://doi.org/10.1016/j.nbd.2019.104619.

73. Hana, S., Peterson, M., McLaughlin, H., Marshall, E., Fabian, A.J., McKissick, O., Koszka, K., Marsh, G., Craft, M., Xu, S., et al. (2021). Highly efficient neuronal gene knockout in vivo by CRISPR-Cas9 via neonatal intracerebroventricular injection of AAV in mice. Gene Ther. *28*, 646–658. https://doi.org/10.1038/s41434-021-00224-2.

74. Kim, J.Y., Grunke, S.D., Levites, Y., Golde, T.E., and Jankowsky, J.L. (2014). Intracerebroventricular viral injection of the neonatal mouse brain for persistent and widespread neuronal transduction. J. Vis. Exp. *51863*, 51863. https://doi.org/10.3791/51863.

75. Wang, M., Misgeld, T., and Brill, M.S. (2022). Neural labeling and manipulation by neonatal intraventricular viral injection in mice. STAR Protoc. *3*, 101081. https://doi.org/10.1016/j.xpro.2021.101081.